Biophysical Chemistry 141 (2009) 1–10

Contents lists available at ScienceDirect

Biophysical Chemistry

journal homepage: http://www.elsevier.com/locate/biophyschem

Equilibrium unfolding of the retinoid X receptor ligand binding domain and characterization of an unfolding intermediate

Mark E. Harder [a,*,1], Dean A. Malencik [a,1], Xuguang Yan [b,d], David Broderick [a], Mark Leid [c,d], Sonia R. Anderson [a,1], Max L. Deinzer [b,d], Michael I. Schimerlik [b,d,1]

[a] Department of Biochemistry and Biophysics, Oregon State University, Corvallis, OR 97331-7305, United States
[b] Chemistry, Oregon State University, Corvallis, OR 97331-7305, United States
[c] College of Pharmacy, Oregon State University, Corvallis, OR 97331-7305, United States
[d] Environmental Health Sciences Center, Oregon State University, Corvallis, OR 97331-7305, United States

ARTICLE INFO

Article history:
Received 4 August 2008
Received in revised form 2 December 2008
Accepted 2 December 2008
Available online 16 December 2008

Keywords:
Retinoid X receptor ligand binding domain
Equilibrium unfolding mechanism
Analytical ultracentrifugation
Fluorescence
Circular dichroism

ABSTRACT

The retinoid X receptor (RXR) is a ligand-activated transcription factor that plays an important role in growth and development and the maintenance of cellular homeostasis. A thermodynamic ultraviolet circular dichroism, tryptophan fluorescence and ligand binding activity with guanidine as a chemical denaturant are consistent with a two step mechanism. The dimeric LBD equilibrates with a monomeric intermediate (ΔG^0 (H_2O) equal to 8.3 kcal/mol) that is in equilibrium with the unfolded state ($\Delta G^0(H_2O)$ equal to 2.8 kcal/mol). The intermediate was characterized by analytical ultracentrifugation, spectroscopy, and collisional fluorescence quenching, which imply that the monomeric intermediate maintains a high degree, but not all, of native secondary structure. Although intrinsic fluorescence from native and intermediate suggests little change in tryptophan environments, fluorescence intensities from fluorescein reporter groups differ significantly between the two structures. Analysis of the collisional quenching results imply that the intermediate is characterized by tryptophans with increased accessibility to small solutes and less overall compactness than the native protein.

1. Introduction

The effects of retinoids on growth and development are mediated through the retinoic acid receptor (RARα, β and γ isoforms) and the retinoid X receptor, RXRα, β and γ [1]. The RAR is activated by both 9-cis- and all-trans-retinoic acid while the RXR is activated by 9-cis-retinoic acid. The RXR exists as a homodimer (MW=2×26,940D, 2×240 amino acid residues) but can function in signal transduction pathways as either a homodimer or as a heterodimer with other members of the nuclear hormone receptor family [2]. The RAR functions in signal transduction exclusively as a heterodimer with the RXR [3]. The members of the nuclear receptor family have a common structural motif [4]: an amino terminal domain (A/B) containing a transactivation function (AF1) followed by a DNA binding domain (DBD) including two zinc fingers (C), a hinge region (D) and a ligand binding domain (LBD or E) with a second activation domain (AF2) located near the carboxyl terminus of the ligand binding domain.

The atomic structures of several members of the nuclear receptor family have been determined [5] including those of the RAR and RXR LBDs [6–11]. Comparison of the X-ray structures in the presence and absence of agonists led to the development of a structural model for agonist action [4,5] in which the binding of an agonist causes movement of helices 11 and 12 with helix 12 covering the bound ligand. The movement of helix 12 and juxtaposition with helices 3, 4 and 5 creates the binding site for transcriptional coactivators. Transient kinetic studies of 9-cis-retinoic acid binding to RXR support this model in that they were consistent with a ligand-induced conformational change in the protein and suggested that the driving force in the binding of the agonist was the large entropy change resulting from the conformational rearrangement [12]. Analysis of the hydrogen-deuterium (H/D) exchange kinetics of the RXR LBD dimer in the presence and absence of 9-cis-retinoic acid generally agreed with the predictions of the X-ray structure although protection by agonist was also found in additional regions of the protein not in direct contact with bound 9-cis-retinoic acid [13].

Little is currently known regarding the folding mechanism of ligand-activated transcription factors. The folding mechanism of the ligand-binding domain of the glucocorticoid receptor showed three states at equilibrium [14] with the folded dimer going to an intermediate dimer, which then unfolded to the denatured monomer. Whether this mechanism is general for all dimeric ligand-activated

* Corresponding author. Department of Biochemistry and Biophysics, ALS2011, Oregon State University, Corvallis, OR 97331-7305, United States. Tel.: +1 541 737 4421, +1 541 602 6398 (cell); fax: +1 541 737 0481.
E-mail address: harderm@onid.orst.edu (M.E. Harder).
[1] Contributed equally to this work.

0301-4622/$ – see front matter © 2009 Elsevier B.V. All rights reserved.
doi:10.1016/j.bpc.2008.12.001

transcription factors is unknown. In addition, it would be of interest to identify and characterize any folding intermediates since they may resemble higher energy, less populated states present in the native ensemble that may be important in the signal transduction process.

Preliminary studies (not shown) indicated that the human RXR dimer at 1 μM concentration could be unfolded and refolded reversibly as indicated by the recovery of the native ultraviolet circular dichroism (CD) and fluorescence spectra after unfolding in 5 M guanidine hydrochloride (GuHCl) and dilution of the unfolded protein to a final guanidine concentration of 0.25 M. Ligand binding activity was also recovered to greater than 95%. This was then used as a model system in the development of a novel method for analyzing spectroscopic data for three state titrations in equilibrium unfolding experiments [15]; however, at that time it was not possible to differentiate between monomeric and dimeric folding intermediates. The quantitative analysis must also be revised since the CD spectra used in those experiments may have been compromised by protein aggregation.

In this manuscript, the equilibrium unfolding mechanism of the human RXR ligand-binding domain is examined by CD and fluorescence spectroscopy and the dependence of 9-cis-retinoic acid binding on denaturant concentration. Thermodynamic parameters are calculated for the observed three state system under conditions in which aggregation is insignificant. The intermediate identified in these studies is characterized by collisional quenching of tryptophan fluorescence and analytical ultracentrifugation. The latter studies were done using both the native receptor at guanidine concentrations sufficient to induce the intermediate and unfolded states and a fluorescently labeled RXRα LBD preparation that could be used at sufficiently low concentrations to determine the monomer–dimer equilibrium constant under aggregation-free conditions. The results of these experiments indicate that the RXR dimer unfolds via an expanded monomeric intermediate containing a high degree of secondary structure and a modestly perturbed environment of the protein tryptophan residues. At higher denaturant concentrations, the intermediate loses secondary structure and the environment of the tryptophans becomes more polar as the protein unfolds.

2. Experimental

2.1. Protein preparation

The pET 15b construct containing the retinoid X receptor ligand binding domain (T226 to T462) was the generous gift of Pierre Chambon (Institute de Genetique et de Biologie Moleculaire et Cellulaire, College de France, Strasbourg, France). Wild-type RXR was expressed and RXR dimers were purified as described previously [13] with the exception that preparations containing over 50 mg of protein were purified by chromatography on a 2.5×65 cm Sephacryl S200 size exclusion column after thrombin cleavage of the hexaHis tag. Protein concentration was determined using the extinction coefficient of 0.58 A_{280}/mg/ml protein [16]. ULTROL grade guanidine hydrochloride was purchased from Calbiochem, 3-[(3-cholamidopropyl)-dimethylammonio]-1-propanesulfonate (CHAPS) from Anatrace, and all other reagent grade material from Sigma-Aldrich. All experiments were done in a buffer consisting of 50 mM potassium phosphate, 0.5 M potassium chloride, 0.5 mM CHAPS, 1 mM tris(2-carboxyethyl) phosphine hydrochloride (TCEP) at 30 °C, pH 7.4. Guanidine stock solution concentrations were determined from the refractive index [17]. The RXRα LBD monomer concentration was 2 μM for the fluorescence and CD experiments and 0.5, 1.5 μM, and 3.5 μM for the analytical ultracentrifuge runs.

2.2. Fluorescein derivatizion of RXR

100 μl of 30.5 mM fluorescein-5-EX succinimidyl ester (Invitrogen) in DMSO was added to 1.2 ml of RXRα LBD (total monomer concentration of 162 μM) in 1.2 ml of 0.1 M sodium carbonate buffer, pH 8.8, 0.2 M NaCl, 1 mM TCEP with stirring. The reaction was stirred at room temperature in the dark for 5 min and then overnight at 4 °C. The labeled protein was then exchanged into 50 mM potassium phosphate buffer, pH 7.4, 0.5 M NaCl, 1 mM TCEP by repeated centrifugation using an Amicon Ultra-15 (5000 MW cut-off) until no color was observed in the filtrate. Protein recovery was greater than 90%. Fluorescein concentration was determined using a molar extinction coefficient at 491 nm of 86,000 and protein concentration using an A_{280} of 0.58/mg/ml after correction for bound dye. The resulting labeling stoichiometry was one dye molecule per RXRα LBD monomer. Mass spectral analysis showed that the labeling was heterogeneous, occurring at the N-terminal glycine residue and lysines 321, 356, 381, 407 and 417 as well as (surprisingly) asparagine 335.

2.3. Spectroscopic studies

Fluorescence emission spectra from 310 to 450 nm were recorded using an SLM 8100C spectrofluorometer with an excitation wavelength of 280 nm and excitation and emission slit widths of 8 nm. Fluorescence emission at 520 nm of the fluorescein labeled protein was collected using excitation at 491 nm and slit widths of 8 nm. Ultraviolet circular dichroism spectra from 320 to 206 nm were obtained using a Jasco J720 spectropolarimeter. In addition to whole CD spectra, ellipticities at 222 nm were measured as a function of guanidine concentration, averaging 3 measurements, each for 1 min. All samples were kept at 30±1 °C during measurements. The binding of 9-cis-retinoic acid as a function of guanidine concentration was measured in a 2 ml volume in a stirred-cell by the quenching of the fluorescence emission at 340 nm using an excitation wavelength of 280 nm. Ligand-binding titrations were performed at a protein concentration of 0.1 μM and ligand concentrations up to 2 μM.

2.4. Analytical ultracentrifugation

Sedimentation experiments were performed in a Beckman Optima XL-A analytical ultracentrifuge. Buffer densities and viscosity corrections were made according to data published by Laue et al. [18]. The partial specific volume of RXR estimated from the protein sequence according to the method of Perkins [19] was 0.744 cm^3/g. Buffers for the sedimentation velocity and equilibrium runs contained 50 mM potassium phosphate, pH 7.4, 500 mM KCl, and 1 mM TCEP. In some cases 2.5 M GuHCl or 0.25 M GuHCl was included for partially denaturing conditions or 5 M GuHCl for fully denaturing conditions.

Sedimentation velocity runs were performed at 28 °C using a four hole AN-60Ti rotor and double-sector charcoal/Epon filled centerpieces. RXR samples with an initial absorbance at 230 nm of 0.8 (~0.2 mg/ml; ~7.4 μM) were centrifuged at 42,000 rpm. Scans were collected using absorbance optics and analyzed by the method of van Holde and Weischet [20], or the enhanced method of van Holde and Weischet [21] as implemented in the UltraScan, v. 9.1 (http://www.ultrascan.uthscsa.edu, [22]. This analysis yields the integral distribution G(s) of diffusion corrected sedimentation coefficients across the sedimentation boundary.

In addition, the data were analyzed by the computer program Sedfit (http://www.analyticalultracentrifugation.com, [23]. This is software for the analysis of analytical ultracentrifuge velocity data files by direct fitting with numerical solutions of the Lamm equation [23]. The Sedfit analysis is now also implemented in Version 9.1 of UltraScan.

Sedimentation equilibrium experiments were performed at 28 °C according to procedures described [24]. Typically, three 120-μl samples of protein (fluorescein labeled RXRα LBD with and without 5 μM retinoic acid) were sedimented to equilibrium at multiple speeds ranging from 15,000 rpm to 25,000 rpm. Multiple loading concentrations ranging between 0.05 and 0.3 OD at 491 nm were measured;

data exceeding 1.0 OD were excluded from the fit. Scans were collected with absorbance optics at a wavelength of 491 nm. The radial step size was 0.001 cm, and each c versus *r* data point was the average of 20 independent measurements. Two scans were taken at each speed. Equilibrium data spanning the concentration range were examined by global fitting using UltraScan software. Equilibrium data were fit to multiple models using global fitting. The most appropriate model was chosen based on the best statistics and on visual inspection of the residual run patterns.

2.5. Analysis of spectroscopic unfolding data

To fit the data sets of CD or fluorescence spectra (corrected for buffer contributions) as a function of guanidine concentration with a thermodynamic model, the intensity-averaged wavelength ($\langle\lambda_j\rangle$) was computed for each spectrum

$$\langle\lambda_j\rangle = \frac{\sum_{i=1}^{n} \lambda_i I_{ij}}{\sum_{i=1}^{n} I_{ij}} \quad (1)$$

where λ_i is the wavelength and I_{ij} is the intensity of the *j*th spectrum at wavelength *i*. Using the same reasoning described in Harder et al. [15], an equation relating the $\langle\lambda_j\rangle$ values to the appropriately weighted matrix of mole fractions of the species in equilibrium can be derived. Least square estimates of the thermodynamic parameters — $\Delta G^0(H_2O)$, the standard free energy change of unfolding in the absence of denaturant, and *m*, the slope of the linear dependence of unfolding free energy change on concentration of denaturant. See below — that determine the mole fraction matrix could be obtained starting with fixed estimates of the signals from each of the three species, minimizing the thermodynamic parameters, then iterating until convergence of the rms errors. The procedures for fitting ellipticities at 222 nm and emission intensities at 335 nm and 520 nm were analogous to those employed for the average fluorescence wavelengths. Once the thermodynamic parameters were obtained, the denaturant dependence of the mole fraction of monomer (*I*), dimer (F_2), and unfolded monomer (*U*) were calculated from the mass action expression for the equilibrium unfolding of the RXRα LBD dimer:

$$F_2 \overset{K}{\rightleftharpoons} 2I \overset{K_U}{\rightleftharpoons} 2U. \quad (2)$$

The mole fraction of each species was calculated from the law of mass action as follows:

$$f_U = 2/\left(a + \sqrt{a^2 + b}\right) \quad (3)$$

where $a = 1 + 1/K_U$ and $b = 8P_{tot}/KK_U^2$

$$f_I = f_U/K_U \quad (4)$$

$$f_{F_2} = 2f_U^2 P_{tot}/KK_U^2. \quad (5)$$

Note that all molar concentrations and mole fractions are defined on a monomer basis, so that:

$$P_{tot} = [I] + [U] + 2[F_2] \text{ and } 1 = f_U + f_I + f_{F_2}. \quad (6)$$

In which case, mole fractions and weight fractions are identical.

2.6. Analysis of denaturant-dependent ligand binding data

The data for the dependence of 9-cis-retinoic acid binding on the concentration of guanidine hydrochloride were analyzed assuming a model which coupled denaturant-induced unfolding of a ligand binding-competent monomer (*I*) with formation of the monomer-ligand complex (IL), as shown in Eq. (7) (*U* is unfolded protein, *L* is the 9-cis-retinoic acid ligand):

$$\text{IL} \overset{K}{\rightleftharpoons} I + L \overset{K_1}{\rightleftharpoons} U + L. \quad (7)$$

In Eq. (7), $K = [L][I]/[\text{IL}]$ and $K_1 = [U]/[I]$. Assuming that the denaturant-induced unfolding of monomers obeyed the linear extrapolation model of Schellman [25], $K_1 = \exp[(m\,[D] - \Delta G^0(H_2O))/RT]$.

An initial value for microscopic dissociation constant for 9-cis-retinoic acid was determined by directly fitting the observed fluorescence intensity (*Y*) in the absence of guanidine as a function of total 9-cis-retinoic acid concentration (L_{tot}):

$$Y = Y_0 - 2c\Delta\varepsilon/\left(d + \sqrt{d^2 - 4c}\right) \quad (8)$$

where

$$c = L_{tot}P_{tot} \text{ and } d = L_{tot} + K + P_{tot}.$$

In Eq. (8), Y_0 is the fluorescence in the absence of 9-cis-retinoic acid; *K*, the dissociation constant for binding of the ligand to a homogeneous class of sites; P_{tot}, the total population of sites and $\Delta\varepsilon$ the difference in fluorescence enhancement between the free and occupied receptor.

The experimentally determined dissociation constant for 9-cis-retinoic acid at each concentration of guanidine was defined as K_{app}. Because its calculation is more robust numerically, the negative logarithm of the experimental and trial values of K_{app} was converted to their negative logarithms, pK_{app}. The nonlinear regression routine, given trial values of the global parameters of the fit – the cooperativity parameter, *m*, the free energy change of unfolding in the absence of guanidine, $\Delta G^0(H_2O)$, and the microscopic ligand dissociation constant, *K* – calculates values of pK_{app} according to Eq. (9):

$$pK_{app} = -(\log_{10} K + \log_{10}(1 + K_1)). \quad (9)$$

Thus, pK_{app} depends directly on *K*, and on the thermodynamic parameters through K_1. At the relatively low concentration of total protein used in this experiment (0.1 μM), the total monomer concentration varied by less than 0.01 μM over the range of guanidine concentrations used in these experiments and was considered a constant. Least square differences between calculated and experimental values of pK_{app} were minimized using the simplex method in Scientist.

2.7. Analysis of collisional quenching

Quenching of protein tryptophan fluorescence by acrylamide and nitrate was nonlinear at 0, 2 M, 5 M guanidine and the data were fit to the modified Stern–Volmer equation which assumes a sphere of action for the quencher [26]:

$$F_0/F = (1 + K_D[Q])\exp(V[Q]). \quad (10)$$

In Eq. (10) *F* and F_0 are the fluorescence in the presence and absence of quencher at concentration [*Q*]. *V* is the volume of the sphere in which quenching occurs (in units of M^{-1}), and K_D is the Stern–Volmer constant for quenching which equals the collisional rate multiplied by the lifetime of the excited state before collision. Eq. (10) was fit by nonlinear regression using Scientist (MicroMath) to estimate K_D and *V* with [*Q*] as the independent variable and F_0/F as the dependent variable. The results were identical whether Marquardt's or Powell's algorithm was used.

3. Results

3.1. Analytical ultracentrifugation

Since the stability of native RXR is related to its oligomerization state, extensive studies of the sedimentation velocity and sedimentation equilibrium of the protein at various concentrations in the native state and in the presence of the denaturant guanidine hydrochloride at a range of concentrations were carried out. A brief example of a Van Holde–Weischet analysis is shown in the supplementary information, Fig. S1.

Typically, sedimentation boundaries were scanned 35 times at 50 equally spaced positions within each boundary; however, points corresponding to poorly sampled baselines and plateaus were discarded. In the experiment shown in Fig. S1, approximately 25% of the collected data was discarded. Values of sedimentation constants were extrapolated to infinite time to correct for diffusion of the protein. In the sample illustrated here, we can see that corrected sedimentation values occur in one cluster. The degree of dispersion in $S_{20,w}$ values seen in this example is commonly reported, and results from a combination of non-ideality and extrapolation error.

Van Holde–Weischet analysis of the sedimentation velocity behavior of RXRα LBD (7.4 μM in RXRα monomers) revealed a sedimentation distribution ranging between 2.0 S (5 M GuHCl), and 2.5 S (2.5 M GuHCl) or a broad distribution of values of sedimentation coefficient up to 6 S in the absence of guanidine, indicating a high degree of heterogeneity in this sample (Fig. 1). In order to obtain molecular weight distributions from sedimentation velocity data, one must show that the molecular species involved are in reversible equilibrium with each other. Reversibility was demonstrated by denaturing a sample in 5.0 M guanidine, then diluting to 0.25 M guanidine and comparing the resulting CD spectrum with that of a sample directly diluted to 0.25 M guanidine. Comparison of the two spectra showed a 90% return to the starting point. Stability of native and fully denatured protein was checked by incubating protein samples in the absence of guanidine and in 5.0 M guanidine overnight at 30 °C and comparing the resulting CD spectra with those of fresh samples. In this case, spectra were again identical within 10%. When an attempt was made to determine the kinetics of refolding by measuring ellipticity changes at 222 nm upon dilution of protein in 5 M guanidine in a stop-flow apparatus (Bio-Logic model SFM-4), it was found that the reaction was complete within 1 ms, the dead-time of the instrument. Also, the change in intrinsic protein fluorescence (at 340 nm when excited at 280 nm) upon addition of protein to a 5 M guanidine buffer was followed in a steady-state fluorimeter. The fluorescence signal came to rest within 10 s. Taken together, these simple checks show that samples of fully folded and unfolded protein were by themselves in a state of reversible equilibrium and that equilibrium between these states can be achieved well within the duration of the sedimentation velocity runs. Others studying proteins that unfold via an equilibrium intermediate (e.g. [27]) have observed that refolding of partially unfolded protein is not fully reversible. In the present case, samples of RXR LBD incubated in 2.5 M guanidine overnight showed visible signs of aggregation. Thus, we take signs of very high molecular weight material in our ultracentrifugation experiments to indicate significant irreversibility on these timescales.

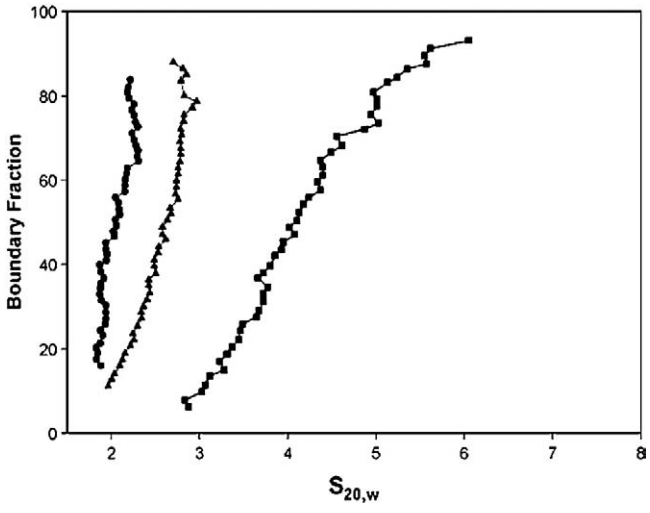

Fig. 1. Sedimentation velocity (42,000 rpm) analysis of RXRα LBD in 50 mM potassium phosphate, 0.5 M KCl, 1 mM TCEP, 0.5 mM CHAPS, pH 7.4. The loading protein concentration was 0.2 mg/ml, corresponding to an absorbance at 230 nm of 0.8. The $G(s)$ plot was obtained through analysis of the sedimentation boundaries by the method of van Holde and Weischet. Filled circles, triangles and squares represent the data for the RXRα in buffers containing 5 M, 2.5 M and 0 M guanidine, respectively.

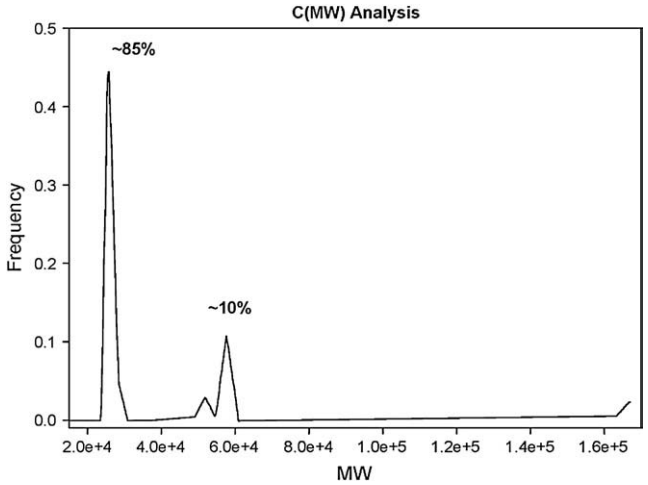

Fig. 2. Analysis of sedimentation velocity (42,000 rpm) of the RXRα LBD in buffer plus 2.5 M guanidine. The total monomer concentration was 7.4 μM. MW is the molecular weight in Daltons.

Sedimentation velocity data were also analyzed by model fitting of the Lamm equation as implemented in Sedfit [23]. The results are illustrated in Figs. 2 and 3, which represent histograms of the molecular weight distribution in the sample. It must be pointed out that lacking knowledge of the frictional coefficients of the species represented in Figs. 2 and 3, these plots are presented for illustrative purposes only. While the information displayed here agrees with

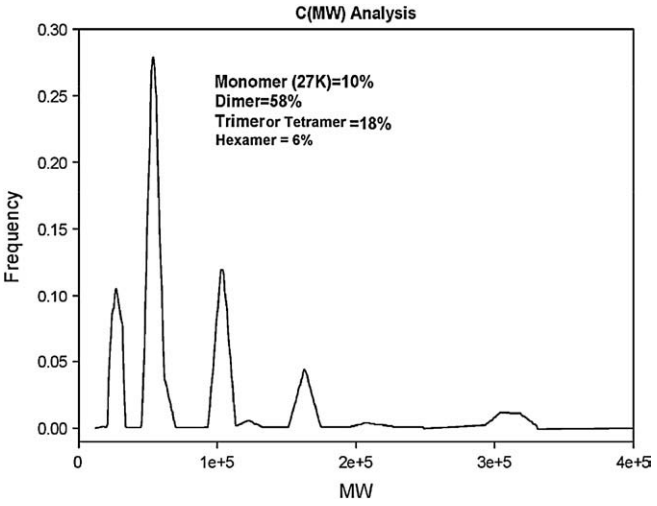

Fig. 3. Analysis of sedimentation velocity (42,000 rpm) of RXRα LBD in buffer in the absence of guanidine. Total monomer concentration was 7.4 μM. MW is molecular weight in Daltons.

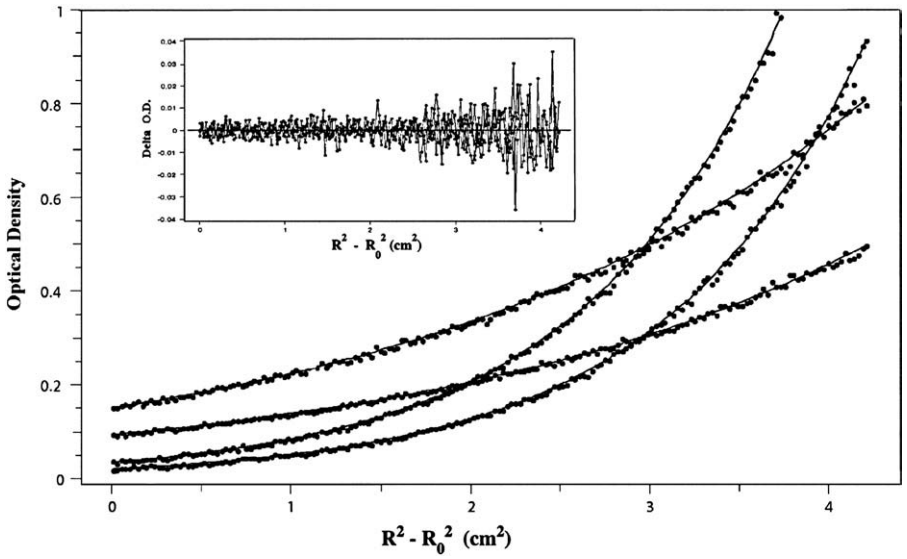

Fig. 4. Sedimentation equilibrium (16,000–27,000 rpm) of unfolded RXRα LBD (2 μM, 3.5 μM) in buffer plus 5 M guanidine. Top panel: fitted overlays (solid lines) to experimental data (filled black circles). Bottom panel: residuals of the fit to a single component model. R = distance from center of rotor to measurement, R_0 = distance to meniscus.

other centrifuge and spectroscopic results, they are not used to derive those results.

All samples analyzed across the concentration range of GuHCl between 0.25 and 2.5 M contained a distribution of putative monomer and dimer (see Fig. 2). In the absence of GuHCl, oligomers of higher degree were observed (Fig. 3). In all sedimentation velocity experiments, which were 5 h in duration, no loss of material by precipitation was detected. In contrast, when sedimentation equilibrium experiments with no GuHCl present were done over a 3 day period, they showed the presence of aggregation and a loss of approximately 40% of the protein. In 5 M GuHCl, the sedimentation equilibrium analyzed as a single ideal species with a molecular weight of ca. 27KD (Fig. 4). In the case of the 2.5 M GuHCl, no loss of protein occurred and the data could be analyzed as having predominately two components, a monomer and a dimer (Fig. 2).

Although a reasonable analysis was obtained for the monomeric intermediate (2.5 M GuHCl) and the unfolded monomer (5 M GuHCl) at 7.4 μM RXRα LBD monomer, it was important to determine whether the native protein was undergoing aggregation at the concentration used for the other unfolding experiments (2.5 μM monomer). Unfortunately, the signal to noise ratio was too low at 230 nm to analyze the analytical ultracentrifuge results for native RXRα LBD monomer at a concentration of 2.5 μM. Thus, further analysis of the monomer–dimer equilibrium under nondenaturing conditions at monomer concentrations less than 3 μM utilized a fluorescein-labeled RXR. This allowed for a protein concentration for sedimentation equilibrium experiments that was similar to those used in the spectroscopic studies. By globally fitting the sedimentation equilibrium data acquired under multiple conditions such as multiple rotor speeds and multiple loading concentrations, it was possible to enhance the confidence in each fitted parameter value. The results of the global analysis are shown in Fig. 5. Parameters such as monomer molecular weight were considered global and were forced to be the same for all included data sets. When a global fit of the data obtained

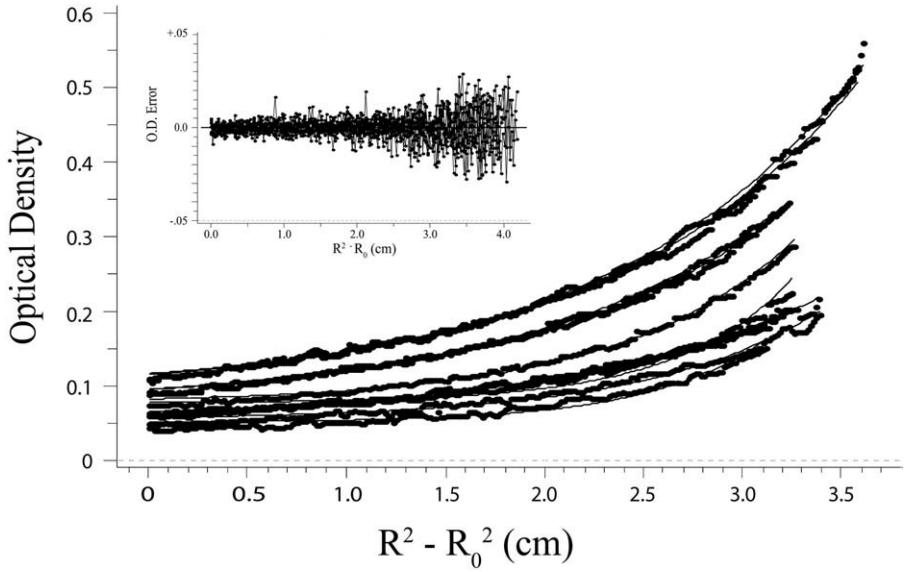

Fig. 5. Global sedimentation equilibrium analysis results for the fluorescein-labeled RXRα LBD. Data were fit to a monomer–dimer model for four speeds (15,000, 18,200, 21,500 and 25,000 rpm) and three loading concentrations (0.5 μM, 1.5 μM and 3 μM monomer) and absorbance was measured at 491 nm. Fitted overlays (solid lines) to the experimental data (black filled circles) are shown in the figure and residuals are shown in the inset. Global analysis of the data sets gave a value of the monomer–dimer dissociation constant equal to 0.832 μM. R and R_0 as in Fig. 4.

Table 1
Sedimentation equilibrium results for studies on RXRα LBD

Equilibrium model	Molecular weight	pK_D
Single ideal species in 5 M GuHCl[a]	27.15 kDa (+0.4/−0.3)	–
Monomer–dimer[b]	27.35 kDa (+3.8/−4.1)	6.1 (+0.9/−1.1)
Monomer–dimer+retinoic acid (5 μM)[b]	26.85 kDa (+4.2/−3.9)	5.9 (+0.9/−0.5)
Calculated from protein sequence[a]	26.94 kDa (monomer)	–

The 95% confidence intervals determined by Monte Carlo analysis are reported in parentheses.
[a] Unlabeled RXRαLBD.
[b] Fluorescein-labeled RXR.

Table 3
Thermodynamic parameters for RXRα LBD unfolding

Parameter/transition	$N_2 \rightleftharpoons 2I$	$I \rightleftharpoons U$
$\Delta G^0(H_2O)$ (kcal/mol)[a]	8.4±0.2	–
$\Delta G^0(H_2O)$ (kcal/mol)[b]	8.4±0.2	2.8±0.5
$\Delta G^0(H_2O)$ (kcal/mol)[c]	–	2.3±0.2
m (kcal/mol/molar)[b]	0.8±0.3	0.9±0.1
m (kcal/mol/molar)[c]	–	1.2±0.1

[a] From equilibrium sedimentation.
[b] From analysis of CD and fluorescence data.
[c] From analysis of the pK_D (app) for 9-cis-retinoic acid binding as a function of guanidine concentration.

from 0 to 6.5 μM RXR monomer was analyzed, the simplest model consistent with the data giving the lowest variance was a monomer–dimer equilibrium. The 95% confidence intervals determined by Monte Carlo analysis and the equilibrium constants are shown in Table 1.

Although RXRα LBD had a tendency to aggregate when subjected to long equilibrium centrifugation runs, it remained in solution in the presence of partially denaturing concentration of guanidine, even at the highest concentrations of total protein used in these studies. This provided an opportunity to compare the association behavior of unlabeled protein at 7.4 μM with that of fluorescein-labeled protein at lower concentrations (0.5–3 μM). The equilibrium constant for dimer dissociation as determined by sedimentation equilibrium of the labeled protein at low concentrations was about 1 μM. Using this value and the fitted thermodynamic data (Tables 2 and 3, see below) for both labeled and unlabeled protein preparations (which were similar) one can calculate that at 2.5 M GuHCl and 7.4 μM total monomer concentration, 85% of the protein should be the monomeric species. As illustrated in Fig. 2, sedimentation velocity experiments under these conditions show that the protein was approximately 85% monomeric, as expected. The remaining protein consisted of dimer and minor species. Thus the observed analytical ultracentrifuge results obtained for the native protein in 2.5 M GuHCl were consistent with the thermodynamic unfolding data obtained for both the native and labeled protein and the monomer–dimer equilibrium constant, which could be obtained in an aggregation-free system only for the labeled protein. This suggests that the value obtained for the monomer–dimer equilibrium dissociation constant of the fluorescein-labeled protein could be applied to the monomer–dimer equilibrium of the native protein as well.

In summary, the concentrations used in the sedimentation equilibrium studies best fit a monomer–dimer equilibrium with a dissociation constant equal to $(8.3\pm1.7)\times10^{-7}$ M as shown for the fluorescently-labeled protein in Fig. 5. Similar experiments done in the presence of 5 μM 9-cis-retinoic acid gave results that were not significantly different than those for unliganded protein (Table 1) indicating that binding of the agonist did not selectively stabilize the dimeric state.

3.2. Spectroscopy

Four spectroscopic probes of structure were employed to follow the loss of native protein structure as a function of guanidine concentration. Measurements from two of these titrations, together with approximations reconstructed using least-squares estimates of model parameters are shown in Fig. 6. Formally analogous to the first moment of a probability distribution, the intensity-weighted mean wavelength locates the center-of-mass wavelength of the spectrum. As such, it reports on the interaction of multiple transition moments of the protein tryptophans (and, to a lesser extent, tyrosines) with solvent dipole moments and with the rest of the protein. Compact forms of proteins with tryptophan residues located in hydrophobic environments show maximum fluorescence at shorter wavelengths compared to unfolded proteins that have their aromatic residues exposed to solvent. The results in Fig. 6A show the increase in intensity-weighted mean wavelength with added guanidine expected of an unfolding protein. A collection of fluorescence spectra is shown in Fig. S2A.

Changes in protein secondary structure were observed by measuring the ultraviolet circular dichroism at 222 nm. The magnitude of this signal relates to the amount of alpha helical secondary structure present in the protein. These results, shown in Fig. 6B, are consistent with the overall loss of secondary structure that accompanies the loss of compactness upon unfolding. Although the presence of an intermediate was not evident in the data in Fig. 6, analysis of the entire CD and fluorescence spectra according to the methods of Harder et al. [15] showed six components: three species and three perturbation spectra. Attempts to fit the data with a two-state model failed to produce reasonable CD and fluorescence spectra corresponding to the folded and unfolded pure species. Given the spectra sampled in Fig. S2A, the three-state model and the derived estimates of $\Delta G^0(H_2O)$ and m for both transitions, the fluorescence spectra of native dimer and intermediate and unfolded monomers were calculated. These are shown in Fig. S2B.

Multisite covalent labeling with fluorescein created protein in which the intensity of fluorescence (emission at 520 nm, excitation at 491 nm) increased upon unfolding (Fig. 7). This may be attributed to

Table 2
Spectroscopic analysis of RXRα LBD equilibrium unfolding

Method	$N_2 \rightarrow 2\ I$		$I \rightarrow U\ 2$		Pure species signals			
	ΔG^0	m	ΔG^0	m	Native	Intermediate	Unfolded	(Units)
[1]CD_{222}	7.50±0.11	0.80±0.27	2.20±0.27	0.94±0.10	−4.00	−2.25	−0.23	mdeg
[2]CD_{222}	8.86±0.15	0.80±0.29	2.46±0.65	0.93±0.10	−4.20	−2.75	−0.30	"
[3]Fluorescence at 520 nm	8.46±0.37	1.76±2.30	4.20±0.39	1.00±0.09	0.70	0.24	1.15	A.U.
[4]Fluorescence at 520 nm	8.47±0.50	1.60±2.19	3.95±0.38	1.02±0.10	0.70	0.20	1.25	"
[5]Fluorescence at 335 nm	7.72±1.96	1.60±6.92	2.31±1.57	0.96±0.08	0.98	1.03	0.31	A.U.
[5]F335 − $\langle I\ \lambda \rangle$	9.61±1.08	0.90±0.39	2.51±0.62	0.92±0.18	348.0	348.0	362.5	nm

Estimated thermodynamic parameters and species signals for spectroscopic titrations. $\langle I\ \lambda \rangle$ are intensity-weighted mean wavelengths of fluorescence spectra. Emission intensities observed at 520 nm are from RXR-LBD labeled with fluorescein (see Methods) excited at 491 nm; 335 nm intensities are from protein tryptophans excited at 280 nm. CD_{222} denotes ellipticity measurements at 222 nm in units of mdeg. Units for standard free energies are kcal mol^{-1}; units for m values are kcal mol^{-1} M^{-1}. Units for species signals are in the last column; A.U. = unitless relative counts. Concentrations of monomeric RXRα LBD have the following values: 2.0 μM, 2.2 μM, 0.1 μM, 1.0 μM, and 2.2 μM for superscripts 1 to 5 respectively.

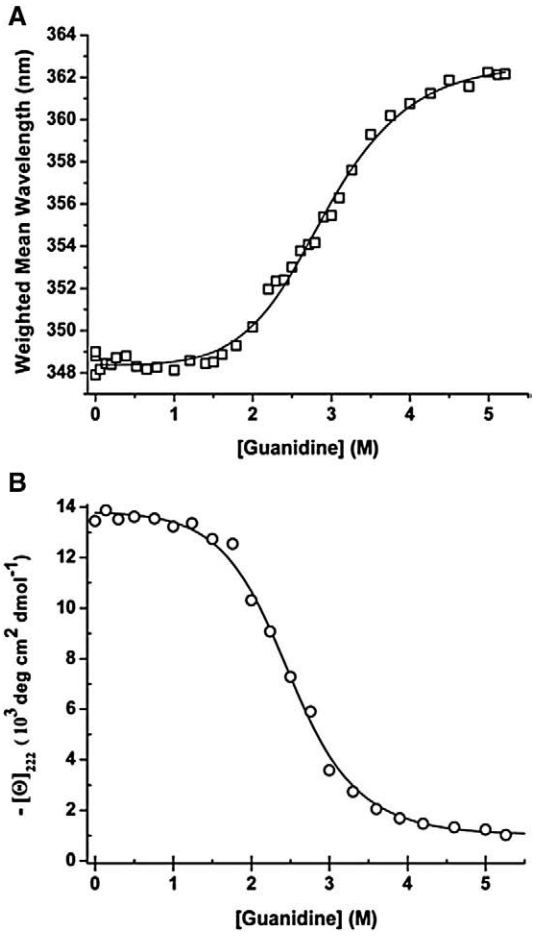

Fig. 6. Spectroscopic data observed and calculated from parameter estimates. Symbols: original data. Lines: Values expected given the estimated thermodynamic parameters and the intensities of the three equilibrium species. All data collected from 2.2 μM RXRα LBD. A. Intensity-weighted mean wavelengths of the fluorescence spectra acquired at the concentrations of guanidine hydrochloride shown on the abscissa were calculated using Eq. (1). Weighted mean wavelengths were calculated from fluorescence spectra and analyzed as described in Experimental. B. Circular dichroic mean residue ellipticities at 222 nm. Ellipticity at 222 nm collected as described in Methods and converted to mean residue ellipticities using pathlength in mm (10.0), concentration in mg/ml (0.05), monomer molecular weight of 27,200 D, and polypeptide chain length of 240 residues.

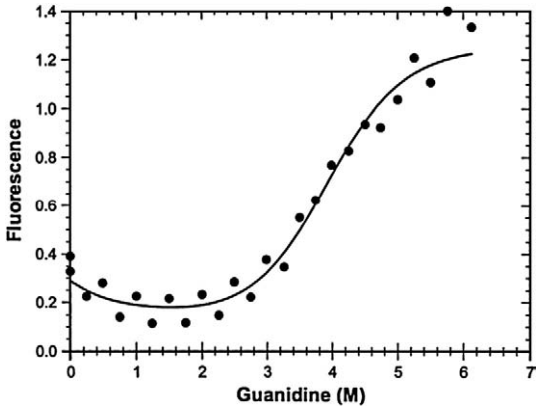

Fig. 7. Dependence of the unfolding of the fluorescein-labeled RXRα LBD on guanidine concentration. Fluorescence intensity at 520 nm was measured as a function of GuHCl concentration. Data (closed circles) were analyzed as described in the Materials and methods section. The fitted parameters and the pure species signals for the fit (solid line) are given in Table 2.

release from fluorescein self-quenching upon loss of tertiary compactness ([28] and citations therein). The joint fit of the fluorescence and circular dichroism unfolding data for the native protein (Fig. 6A,B) agrees quite well with the fit of the unfolding data of the protein heterogeneously labeled with fluorescein used for the ultracentrifuge studies (Fig. 7).

Estimates of the thermodynamic and spectroscopic parameters from all these titrations are summarized in Table 2. These data include

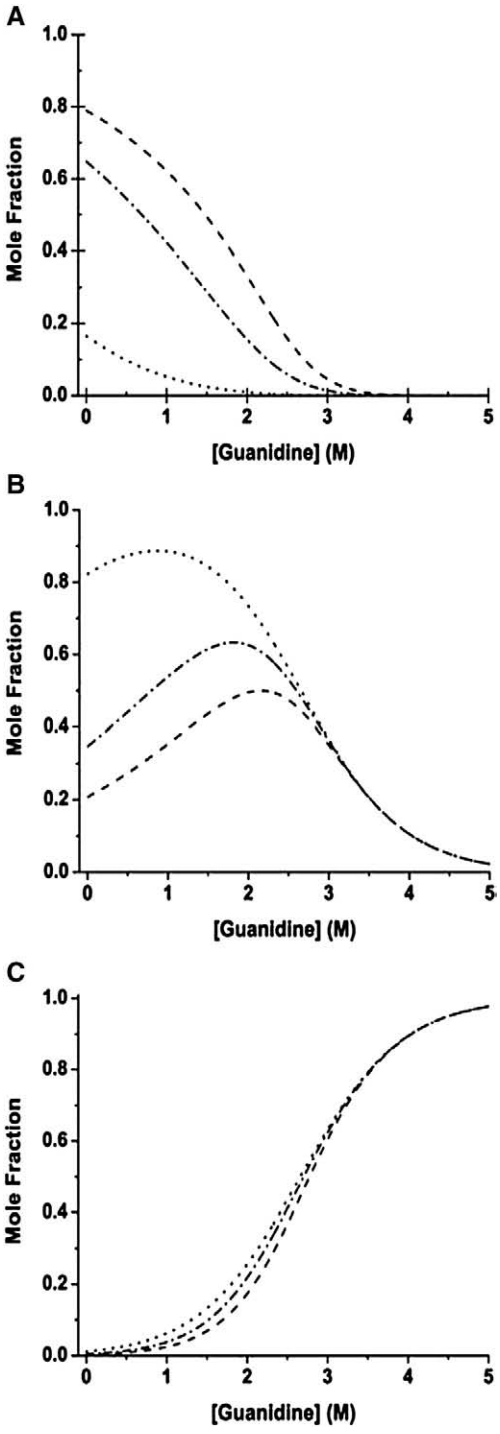

Fig. 8. Species mole fractions versus guanidine concentration. Using estimates of the thermodynamic parameters (Table 3), the mole fractions of native dimer (A), monomeric intermediate (B) and unfolded protein (C) were calculated from Eqs. (2)–(6) as described in Methods at 3 different RXR concentrations: 0.1 μM, 2.2 μM, and 7.5 μM (dotted, dash-dotted and long dash, respectively).

unfolding results from two independent CD experiments and evaluation of the fluorescence intensity and intensity-weighted mean wavelength for the native protein as well as two independent experiments fitting the fluorescence intensity and intensity-weighted mean wavelength data for the flourescein-labeled protein. The comparative effects of the native-to-intermediate and intermediate-to-unfolded transitions on secondary and tertiary structure can be judged from estimates of the pure species signals. The ellipticities at 222 nm of native and intermediate species were identical, but almost completely disappeared in the case of the unfolded protein. Fluorescence intensity at 335 nm and intensity-weighted average wavelength behaved similarly in that the native and intermediate species are characterized by nearly equal signals, followed by a large change going to the unfolded form. In the labeled protein, the intensity of fluorescein fluorescence from the intermediate was the smallest of the three forms. If the strength of this signal was inversely related to fluorescein self-quenching, it would imply that critical fluorescein moieties quenched most strongly in the intermediate folding state. Because the label was distributed over several side-chains, a more complete analysis is not possible at this time, but this result suggests that some of the labeled residues are closer in the unfolding intermediate than in the native form.

Estimates of standard errors were also derived, and using the inverses of these as weights, globally derived mean values for the thermodynamic parameters were calculated, as reported in Table 3. Using these, the mole fractions of each species as a function of guanidine and total protein concentrations were calculated. The strong protein concentration dependence of the expected concentrations of the native dimer and the monomeric intermediate at guanidine concentrations less than 2 M is shown in the first two panels of Fig. 8.

Since the spectroscopic data were consistent with two transitions, a second approach using a different signal was attempted. The dissociation constant of 9-cis-retinoic acid was found to be dependent on guanidine concentration (Fig. 9). On the logarithmic scale, which is proportional to free energy, the transition in the dissociation constant spans more than 2 orders of magnitude, centered at approximately 2 M guanidine. The free energy of ligand binding is essentially unchanged up to 1 M guanidine. Calculation of the mole fraction of dimer from the data in Table 3 at a concentration of 0.2 μM total RXRα LBD shows that it decreases from 0.3 to 0.1 as the GdnHCl concentration goes from zero to 1 M. Thus one can infer that it is the conversion of the monomeric intermediate to the unfolded form which accounts for the major loss of ligand affinity.

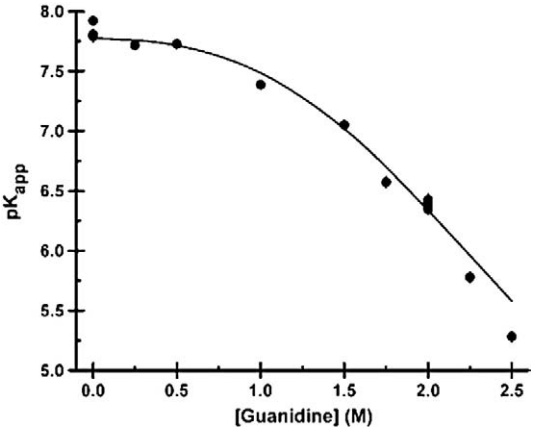

Fig. 9. Dependence of the apparent dissociation constant for 9-cis-retinoic acid on guanidine concentration. The apparent dissociation constant for 9-cis-retinoic acid was determined at each guanidine concentration from a fit of the fluorescence quenching data with Eq. (8). All experiments were done at a RXR monomer concentration of 0.2 μM. Values of the pK_{app} were fit with the model in Eq. (6) as described in Methods and the solid line is the fitted curve. The parameters calculated from the fit are given in Table 2. Vertical bars are standard errors.

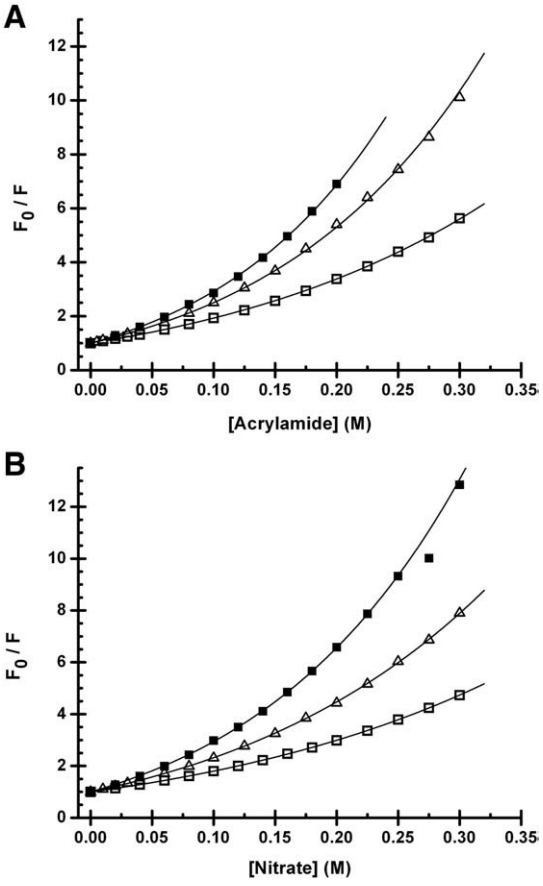

Fig. 10. Collisional quenching as a function of guanidine concentration. Tryptophan fluorescence was measured (Methods) as a function of the concentration of two quenching agents in the presence of guanidine hydrochloride at three concentrations — 0 M (open squares), 2.5 M (triangles), and 5 M (filled squares). A: quenching by acrylamide. B: quenching by sodium nitrate.

Assuming that the first transition (to a monomeric intermediate) resulted in no change in affinity for ligand – an approximation supported by the independence of sedimentation behavior on the presence of saturating concentrations of ligand – the denaturant-dependence of pK_{1app} (Fig. 9) was determined and the data fit with the unfolding model as described in the Methods section. The estimated values of $\Delta G^0(H_2O)$, and m for the second transition agreed with the spectroscopic analysis, further supporting the proposed model and validity of the thermodynamic parameters.

In order to examine the changes in accessibility of the two tryptophan residues per monomer to fluorescence quenching, acrylamide and nitrate were used as collisional quenchers. The observed quenching was nonlinear and the data were fit to Eq. (10) (Methods). Fig. 10 shows experimental data and curves of F_0/F calculated from the fitting procedure. The estimated parameters, summarized in Table 4,

Table 4
Fluorescence quenching of RXRα LBD as a function of denaturant concentration

Quencher	Guanidine (M)	K_D (1/M)	V (M)
$NaNO_3$	0	3.86±0.04	2.62±0.03
	2.5	6.95±0.08	3.13±0.03
	5.0	9.62±0.15	4.04±0.06
Acrylamide	0	4.35±0.06	2.96±0.03
	2.5	6.42±0.17	4.21±0.08
	5.0	7.89±0.29	4.90±0.14

show that both the quenching constant, K_D, and the quenching volume, V, increased 2–3 fold in going from the native to the unfolded state, with intermediate values for equal mixtures of monomeric and unfolded RXR.

4. Discussion

The goals of these experiments were to evaluate the equilibrium unfolding mechanism of the RXR homodimer, calculate the free energy changes for each step in the pathway and, if possible, characterize any equilibrium unfolding intermediates. The experiments were complicated by the tendency of the protein to aggregate at 30 °C at concentrations higher than 80 μg/ml (about 3 μM in total RXR monomer). Fluorescence and CD spectra appeared stable under the conditions used in most experiments (2 μM) although the low protein concentrations did result in lower signal to noise ratios in the observed CD. The sensitivity of the analytical ultracentrifuge was such that higher protein concentrations were required (7.4 μM) unless it was labeled with fluorescein, in which case sedimentation boundaries and gradients could be measured at total protein concentrations as low as 0.5 μM. Although the analytical ultracentrifuge experiments for the native protein were complicated by the presence of higher molecular weight species, they were generally interpretable in terms of the molecular weight distributions of monomer and dimer in solution.

Formally, the data could be analyzed in terms of either a monomer (I) or dimer (I_2) intermediate which could be on the folding pathway:

$$F_2 \overset{K}{\rightleftharpoons} 2I \overset{K_U}{\rightleftharpoons} 2U \text{ or } F_2 \overset{K}{\rightleftharpoons} I_2 \overset{K_U}{\rightleftharpoons} 2U \tag{11}$$

or off-pathway:

$$2I \overset{K}{\rightleftharpoons} F_2 \overset{K_U}{\rightleftharpoons} 2U \text{ or } I_2 \overset{K}{\rightleftharpoons} F_2 \overset{K_U}{\rightleftharpoons} 2U. \tag{12}$$

When the distribution of species as a function of denaturant concentration was calculated (Fig. 8), the intermediate state dominated at 2 M guanidine. Analytical ultracentrifugation experiments showed that in the absence of guanidine, at an RXRα LBD monomer concentration of 7.4 μM, the protein was mainly a dimer with the presence of some tetrameric and higher order aggregates of protein (Fig. 3). At 2 M guanidine, the monomer was the main species present at low and high concentrations of protein. The unfolded species at 5 M guanidine was a monomer in all cases. Thus, the intermediate was considered to be the RXR monomer.

The on pathway mechanism involves a progression through a series of less-folded states, while the off pathway mechanism involves the interposition of the dimeric state between the two monomeric states. Thus, at high denaturant concentrations, the partially unfolded intermediate state could be in equilibrium with the fully unfolded state only by regaining quaternary and partial tertiary structure prior to unfolding. Even if this dimeric intermediate consisted of largely unfolded subunits, it is difficult to propose a reasonable structural explanation for the requirement that monomers created by denaturing solvent conditions would have to re-associate in order to unfold completely at still higher concentrations of denaturant. Therefore, we consider the on-pathway mechanism to be more likely in the absence of theoretical and experimental justifications for the more elaborate off-pathway mechanism.

The values of $\Delta G^0(H_2O)$ and m (Tables 2, 3) determined from fitting the on-pathway unfolding model to the spectroscopic data for both native and fluorescein-labeled protein agreed well with those determined using ligand binding as a probe for the folded to monomer intermediate transition (Fig. 9, Table 3). The values for the thermodynamic parameters suggest that the free energy change for the first transition (folded dimer to intermediate monomer, 8.4 kcal/mol) is more than 3 times that for the second transition (monomer intermediate to unfolded monomer, 2.3–2.8 kcal/mol). The values of m are roughly equal (~0.8 versus ~1 kcal mol^{-1} M^{-1}). If one accepts the structural interpretation that values of m correlate with degrees of change in solvent exposure [29], then it would appear that the formation of partially unfolded monomers accounts for 80% of the energy change of unfolding and about half of the average change in time-averaged solvent exposure. Additionally, fluorescence quenching data support an expanded, nonnative intermediate structure. Thus, the tryptophan residues are more exposed to solution than in the folded dimer. Measurements of ellipticity at 222 nm as a function of guanidine concentration, which are chiefly diagnostic for the contribution of alpha helix to secondary structure, suggest that the intermediate retains significant secondary structure that was present in the native dimer.

Results of unfolding 20 dimeric proteins have been reviewed and compared by Neet and Timm [30], who find that overall standard free energy changes of unfolding of proteins of at least 100 amino acid residues range from 13 to 27 kcal/mol, or 0.13 to 0.22 kcal/mol residue. Compared with these figures, the overall standard free energy change for unfolding the RXR ligand binding domain is unusually low — 8.3 + 2 (2.8) = 13.9 kcal/mol, or 0.057 kcal/residue. If this lack of stability characterizes the entire receptor protein, then the latter must exist primarily as a monomer at sub-micromolar concentrations and thus be available for association with other nuclear proteins with little energy cost. Otherwise, control of the state of association of RXRα with other nuclear receptors resides in the other domains.

Guanidine, rather than urea, was chosen as the denaturing agent because it denatured RXR over a greater range of concentrations. In the case of this protein, and probably many others that unfold through more than one transition, the resolution of multiple equilibrium species is greater when the choice of denaturant results in a longer span of denaturant concentrations. However, the authors are aware that this choice complicates the interpretation of unfolding results. Guanidine is charged; urea is not. In the former case, then, salt effects should change in magnitude when guanidine concentration is increased. The effect of guanidine on pH was checked by pH meter and with pH paper. The pH change over the range of guanidine concentration was within 0.5 pH units by either method. Possibly, the inclusion of 0.5 M KCl in the guanidine stock solution prior to adjusting its pH raised the background chloride effects at least through the lower range of guanidine concentration. More general but less understood salt effects on the stabilities of protein species have been reported in the methodological literature (for example [31] and [32]).

But these effects are far from universal. Makhatadze [31] finds that guanidine has a pronounced *stabilizing* effect on ubiquitin at less than 0.5 M denaturant. On the other hand, guanidine destabilizes a different protein, oxidized *E. coli* thioredoxin, throughout the concentration range of the single unfolding transition [32], although there is a deviation from linear dependence of this negative free energy change below 1.5 M guanidine. In contrast to both these studies, Dignam et al. [27], using silkworm glycyl-tRNA synthetase as a model system for three-state unfolding reach a different conclusion. They compared the stabilities of this protein towards urea and guanidine and found that without taking precautions, such as maintaining a constant concentration of chloride across the guanidine unfolding titration, the stabilities of the folding intermediate in the two denaturants are identical within the limits of error. In contrast, they find that the calculated free energy changes of unfolding of the native protein, which are quite small, do depend on the choice of denaturant. Thus, in the absence of any theoretical justification, there does not seem to be any *a priori* reason for assuming that nonlinearity of the response of protein stability to denaturant concentration is universal, nor is their any way to predict the degrees of nonlinearity, even among the different transitions of a given multiple-state unfolder.

While the nonlinear effects cannot be discarded, we believe that our analytical methods, which differ from that of the above studies, at the very least ameliorate these effects [15]. It is a common observation, one that is apparent in some of the aforementioned studies, that there is an apparently linear dependence of spectroscopic magnitudes on denaturant concentration in the zone below the first transition. Compared with urea, this effect is generally greater when guanidine is used as denaturant (for example, see Fig. 1 in [32]. In the method of analysis employed here [15] this apparent stabilization of the protein is treated as an intrinsic feature of the model, and therefore compensated by the method of data analysis. This has the effect of shifting the midpoint of the transition to lower denaturant concentrations, which reduces the tendency of the simple linear extrapolation method to exaggerate the stability of the native species.

One must also be cognizant that all the probes used in these studies are low-resolution in that they report on aspects of global structure — secondary structure, state of association, tryptophan environments, and solvent protection. It is always possible that the addition of yet another technique to the study of RXR ligand binding domain unfolding could reveal a third transition which is silent with respect to the probes employed here. Thus, the three-state model presented here should be regarded as a minimal one, since more complicated unfolding equilibria have not been ruled out.

In summary, the equilibrium unfolding mechanism of the dimeric ligand binding domain of the retinoid-X receptor was examined at 30 °C using the chemical denaturant guanidine. The results were consistent with a model in which the folded dimer goes to an on-pathway intermediate monomer that binds ligand and is much less compact in structure. The largest free energy change and a moderate change in solvent accessibility are observed in this transition. The intermediate then goes to the unfolded state which is characterized by loss of most, if not all, of the correlated secondary structure and the remainder of the shielding of hydrophobic core residues from solvent.

Acknowledgements

The authors would like to acknowledge the support of USPHS grants P30 ES00210, ES00040 and DK060613 and the Oregon State University Foundation (SRA). The authors would also like to acknowledge the assistance of the Molecular Structure and Interactions and Mass Spectrometry Facilities and Services Cores of the Oregon State University Environmental Health Sciences Center and the Oregon State University Foundation. We Thank Dr. Borries Demeler at the Bioinformatics Core Facility at the University of Texas Health Science Center in San Antonio for providing access to the UltraScan LIMS (http://uslims.uthscsa.edu). We also acknowledge Dr. Pierre Chambon for the generous gift of the expression plasmid for RXR, and Susan Perkins and Barbara Hanson for their computer and word processing assistance in the production of this manuscript.

Appendix A. Supplementary data

Supplementary data associated with this article can be found, in the online version, at doi:10.1016/j.bpc.2008.12.001.

References

[1] P. Chambon, A decade of molecular biology of retinoic acid receptors, FASEB J. 10 (1996) 940–954.
[2] F. Rastinejad, Retinoid X receptor and its partners in the nuclear receptor family, Curr Opin. Struct. Biol. 11 (2001) 33–38.
[3] P. Kastner, M. Mark, N. Ghyselinck, W. Krezel, V. Dupe, J.M. Grondona, P. Chambon, Genetic evidence that the retinoid signal is transduced by heterodimeric RXR/RAR functional units during mouse development, Development 124 (1997) 313–326.
[4] P.F. Egea, B.P. Klaholz, D. Moras, Ligand–protein interactions in nuclear receptors of hormones, FEBS Lett. 476 (2000) 62–67.
[5] A.C. Steinmetz, J.P. Renaud, D. Moras, Binding of ligands and activation of transcription by nuclear receptors, Ann. Rev. Biophys. Biomol. Struct. 30 (2001) 329–359.
[6] W. Bourguet, M. Ruff, P. Chambon, H. Gronemeyer, D. Moras, Crystal structure of the ligand-binding domain of the human nuclear receptor RXR-alpha, Nature 375 (1995) 377–382.
[7] J.P. Renaud, N. Rochel, M. Ruff, V. Vivat, P. Chambon, H. Gronemeyer, D. Moras, Crystal structure of the RAR-gamma ligand-binding domain bound to all-trans retinoic acid, Nature 378 (1995) 681–689.
[8] W. Bourguet, V. Vivat, J.M. Wurtz, P. Chambon, H. Gronemeye, D. Moras, Crystal structure of a heterodimeric complex of RAR and RXR ligand-binding domains, Mol. Cell 5 (2000) 289–298.
[9] P.F. Egea, A. Mitschler, N. Rochel, M. Ruff, P. Chambon, D. Moras, Crystal structure of the human RXRalpha ligand-binding domain bound to its natural ligand: 9-cis retinoic acid, EMBO J. 19 (2000) 2592–2601.
[10] R.T. Gampe Jr., V.G. Montana, M.H. Lambert, G.B. Wisely, M.V. Milburn, H.E. Xu, Structural basis for autorepression of retinoid X receptor by tetramer formation and the AF-2 helix, Genes Dev. 14 (2000) 2229–2241.
[11] J.D. Love, J.T. Gooch, S. Benko, C. Li, L. Nagy, V.K. Chatterjee, R.M. Evans, J.W. Schwabe, The structural basis for the specificity of retinoid-X receptor-selective agonists: new insights into the role of helix H12, J. Biol. Chem. 277 (2002) 11385–11391.
[12] M.I. Schimerlik, V.J. Peterson, P.D. Hobbs, M.I. Dawson, M. Leid, Kinetic and thermodynamic analysis of 9-cis-retinoic acid binding to retinoid X receptor alpha, Biochemistry 38 (1999) 6732–6740.
[13] X. Yan, D. Broderick, M.E. Leid, M.I. Schimerlik, M.L. Deinzer, Dynamics and ligand-induced solvent accessibility changes in human retinoid X receptor homodimer determined by hydrogen deuterium exchange and mass spectrometry, Biochemistry 43 (2004) 909–917.
[14] S.H. McLaughlin, S.E. Jackson, Folding and stability of the ligand-binding domain of the glucocorticoid receptor, Protein Sci. 11 (2002) 1926–1936.
[15] M.E. Harder, M.L. Deinzer, M.E. Leid, M.I. Schimerlik, Global analysis of three-state protein unfolding data, Protein Sci. 13 (2004) 2207–2222.
[16] P.F. Egea, N. Rochel, C. Birck, P. Vachette, P.A. Timmins, D. Moras, Effects of ligand binding on the association properties and conformation in solution of retinoic acid receptors RXR and RAR, J. Mol. Biol. 307 (2001) 557–576.
[17] Y. Nozaki, The preparation of guanidine hydrochloride, Methods Enzymol. 26 (PtC) (1972) 43–50.
[18] T.M. Laue, B.D. Shah, T.M. Ridgeway, S.L. Pelletier, Computer-Aided Interpretation of Analytical Sedimentation Data for Proteins, Royal Society of Chemistry, Cambridge, 1992, p. 644.
[19] S.J. Perkins, Protein volumes and hydration effects. The calculations of partial specific volumes, neutron scattering matchpoints and 280-nm absorption coefficients for proteins and glycoproteins from amino acid sequences, Eur. J. Biochem. 157 (1986) 169–180.
[20] K.E. van Holde, W.O. Weischet, Boundary analysis of sedimentation-velocity experiments with monodisperse and paucidisperse solutes, Biopolymers 17 (1978) 1387–1403.
[21] B. Demeler, K.E. van Holde, Sedimentation velocity analysis of highly heterogeneous systems, Anal. Biochem. 335 (2004) 279–288.
[22] B. Demeler, UltraScan Software, University of Texas Health Science Center at San Antonio, Department of Biochemistry, 2004 www.ultrascan.uthscsa.edu.
[23] P. Schuck, Size-distribution analysis of macromolecules by sedimentation velocity ultracentrifugation and Lamm equation modeling, Biophys. J. 78 (2000) 1606–1619.
[24] J. Ausio, D.A. Malencik, S.R. Anderson, Analytical sedimentation studies of turkey gizzard myosin light chain kinase and telokin, Biophys. J. 61 (1992) 1656–1663.
[25] J.A. Schellman, Solvent denaturation, Biopolymers 17 (1978) 1305–1322.
[26] J.R. Lakowicz, Principles of Fluorescence Spectroscopy, 2 ed.Plenum Publishers, NY, 1999.
[27] J.D. Dignam, X. Qu, J.B. Chaires, Equilibrium unfolding of *Bombyx mori* Glycyl-tRNA synthetase, J. Biol. Chem. 276 (2001) 4028–4037.
[28] X. Zhuang, T. Ha, H.D. Kim, T. Centner, S. Labeit, S. Chu, Fluorescence quenching: a tool for single-molecule protein-folding study, Proc. Natl. Acad. Sci. U.S.A. 97 (2000) 14241–14244.
[29] J.K. Myers, C.N. Pace, J.M. Scholtz, Denaturant *m* values and heat capacity changes: relation to changes in accessible surface areas of protein unfolding, Protein Sci. 4 (1995) 2138–2148.
[30] K.E. Neet, D.E. Timm, Conformational stability of dimeric proteins: quantitative studies by equilibrium denaturation, Protein Sci. 3 (1994) 2167–2174.
[31] G.I. Makhatadze, Thermodynamics of protein interactions with urea and guanidinium hydrochloride, J. Phys. Chem. B 103 (1999) 4781–4785.
[32] M.M. Santoro, D.W. Bolen, A test of the linear extrapolation of unfolding free energy changes over an extended concentration range, Biochemistry 31 (1992) 4901–4907.